Monte Carlo Simulations of Diffusion in a Coulomb Potential. Applications to Chemically Induced Dynamic Nuclear Polarization (CIDNP)

Martin Goez* and Rainer Heun

Fachbereich Chemie, Martin-Luther-Universität Halle-Wittenberg, Kurt-Mothes-Strasse 2, D-06120 Halle/Saale, Germany

Received: July 5, 2001; In Final Form: August 31, 2001

The diffusion of radical ion pairs was investigated by Monte Carlo simulations of diffusional trajectories using the drift-field approximation and an efficient algorithm for the generation of isotropic diffusional steps. The Fourier cosine and sine transforms of the conditional probability density of first reencounter, which are central quantities in the Freed−Pedersen theory for the calculation of absolute CIDNP intensities, were first obtained numerically. On the basis of these data, and by making use of the characteristic properties of the transforms, model functions were then derived, which approximate both transforms with a negligible error over the range of parameters relevant for CIDNP; six global constants suffice to calculate both sine and cosine transforms.

Chemically induced dynamic nuclear polarization (CIDNP)[1] is an intriguing experimental phenomenon: the formation of nonequilibrium populations of the nuclear spin states in the products of a chemical reaction, which manifest themselves by anomalous NMR line intensities. CIDNP experiments can be used to probe many important aspects of a chemical reaction, and often yield information that is difficult to obtain by other methods.

In the vast majority of cases, CIDNP arises by the radical pair mechanism.[2] The eigenfunctions of a two-radical system are singlet or triplet as long as the spin Hamiltonian is completely dominated by the exchange interaction, in other words, as long as the two radicals reside near each other. Hence, a radical pair is born—which occurs by a chemical reaction such as homolytical bond cleavage or electron transfer, or by chance encounters of two radicals—with a correlation of the electron spins of the two radicals.

After generation of the pair, the two spin-correlated radicals diffuse apart. As soon as their separation exceeds a few molecular diameters, the spin Hamiltonian is completely dominated by the Zeeman and hyperfine interactions of the individual radicals despite the smallness of these interactions, because the exchange interaction decreases very strongly with increasing distance. The eigenfunctions of this system are two doublets. While singlet and triplet may still be used as basis functions under these circumstances, their coefficients in a linear combination become time-dependent because two independent electron spins in a magnetic field (of the NMR spectrometer used for observation in a CIDNP experiment) obviously possess different precession frequencies unless the two radicals are exactly identical (not only chemically but also with respect to the spin state of every magnetically coupled nucleus). This differential precession with a rate that is modified by the nuclear spin state causes the system to evolve into a coherent superposition state, and is the mechanism of intersystem crossing of radical pairs.

Intersystem crossing is only detectable if the electron spin states of the two radicals can be gauged against each other. This occurs by itself when the same two radicals reencounter: As they approach each other, the exchange interaction rises sharply and maps the superposition state onto the eigenstates singlet or triplet. Diffentiation between these is accomplished by electron-spin selective chemical reactions of the radicals with each other. Very frequently, the triplet pair is nonreactive in such a geminate reaction, and triplet pairs ultimately end up by reactions that involve other species, e.g., the solvent. Starting with an ensemble of radical pairs of specific electron spin multiplicity, those nuclear spin states that increase the intersystem crossing rate are thus depleted in the products formed from pairs of that multiplicity, and enriched in the products from pairs of the other multiplicity. This nuclear spin sorting is detected by NMR.

Evaluation of CIDNP measurements frequently relies on calculations of CIDNP effects from magnetic and diffusional parameters. The present work is based on the Freed−Pedersen theory[3] of absolute CIDNP intensities. Central quantities in this theory are the Fourier sine and cosine transforms of the conditional probability density of first reencounter $f(t,d|r_0)$, which describes the probability that two radicals initially separated by distance r_0 (not necessarily the encounter distance) attain a separation d between t and $t + \mathrm{d}t$ for the first time. For freely diffusing radical pairs closed-form expressions for $f(t,d|r_0)$ exist.[4,5] However, in the presence of a Coulombic attraction between the radicals—which is a very important case because it is realized with most radical pairs generated by electron transfer—the only known solutions are infinite series[6] or approximations (see, e.g., ref 7) that cannot be incorporated into the Freed−Pedersen formalism.

In this paper, we perform Monte Carlo simulations of diffusional trajectories to obtain $f(t,d|r_0)$ for radical pairs with a Coulombic attraction between the radicals. Two potential advantages of this approach are a physically transparent implementation, and the facile adaptation to diverse constraints; on these grounds, we chose the Monte Carlo method with a view to future extensions, e.g., to micellar systems, although in the case of unrestricted diffusion it is less efficient than are other methods[8] for computing $f(t,d|r_0)$. By analyzing the numerical Fourier transforms and making use of their

* To whom correspondence should be addressed.

10.1021/jp012537k CCC: $20.00
Published on Web 10/16/2001

characteristic properties, we derive approximation formulas that should allow quite accurate calculations of absolute CIDNP intensities with the Freed−Pedersen theory, and possess functional forms that are expected to be similar to those of the (unknown) exact solutions.

Results and Discussion

Freed−Pedersen Theory of Absolute CIDNP Intensities. Only mixing of the states $|S\rangle$ and $|T_0\rangle$ is considered here, because for most CIDNP experiments this is the only intersystem crossing pathway. The density matrix of an ensemble of radical pairs can be factored accordingly, and the relevant submatrix can be further reduced to three elements, because the total population $\rho_{SS} + \rho_{T_0T_0}$ remains constant during a diffusional excursion as long as chemical reactions with a scavenger or electron spin relaxation involving the other triplet functions are absent. It is advantageous to use the linear combinations $\rho_{SS} - \rho_{T_0T_0}$, $2\mathrm{Re}(\rho_{ST_0})$, and $2\mathrm{Im}(\rho_{ST_0})$ as basis, because the first two correspond to observables, namely, population difference and electron spin polarization. With these variables, the time-evolution of the density matrix under the combined influence of a constant exchange interaction J and a constant mixing matrix element Q occurs according to

$$\frac{\partial}{\partial t}\begin{pmatrix}\rho_{SS}-\rho_{T_0T_0}\\ 2\mathrm{Im}(\rho_{ST_0})\\ 2\mathrm{Re}(\rho_{ST_0})\end{pmatrix}=\begin{pmatrix}0 & -2Q/\hbar & 0\\ 2Q/\hbar & 0 & -2J/\hbar\\ 0 & 2J/\hbar & 0\end{pmatrix}\cdot\begin{pmatrix}\rho_{SS}-\rho_{T_0T_0}\\ 2\mathrm{Im}(\rho_{ST_0})\\ 2\mathrm{Re}(\rho_{ST_0})\end{pmatrix} \quad (1)$$

The matrix element Q of $|S\rangle - |T_0\rangle$-mixing is given by

$$Q=\frac{1}{2}(\Delta g\beta B_0+\sum_i a_i m_i-\sum_k a_k m_k) \quad (2)$$

where $\Delta g\beta B_0$ is the difference of the EPR Zeeman energies of the two radicals, and the sum terms are the hyperfine energies for given nuclear spin states, the first sum pertaining to the first radical. Interchanging the order of the radicals merely inverts the sign of Q.

Expressions describing diffusion, relaxation and chemical reactions can be added to eq 1 (or, if necessary, a more complete version of it that includes also other components of the density matrix) to give the stochastic Liouville equation (SLE).[1c] With the Monte Carlo method, this can obviously be implemented in a physically transparent, and moreover, in a very straightforward way, because for sufficiently small diffusional steps, all differentials may be replaced by finite differences, and quantities such as J and Q may be regarded as constant during a step.

Instead of solving the full SLE, the Freed−Pedersen theory makes use of the concept of an exchange region, which provides a computationally much simpler approach, and even yields analytical results in the case of free diffusion. Owing to the strong distance dependence of J the transition between a spin Hamiltonian that is completely dominated by J and one that is completely dominated by Q takes place within a very small range of distances. As eq 1 shows, only electron spin polarization $2\mathrm{Re}(\rho_{ST_0})$ and phase correlation $2\mathrm{Im}(\rho_{ST_0})$ are mixed in the region where $|J| \gg |Q|$ (the exchange region); moreover, these components of the density matrix are randomized quite rapidly in that region. Outside the exchange region, only population difference $\rho_{SS} - \rho_{T_0T_0}$ (i.e., the quantity detected in a CIDNP experiment) and phase correlation are mixed because $J \approx 0$. Some randomization of these components occurs through the statistical distribution of times spent in this region, but is much slower than is randomization within the exchange region because quite different sizes of the mixing interactions are involved in these two cases.

A diffusional excursion is assumed to start at an interradical separation r_0 where J becomes negligible, and with zero electron spin polarization and phase correlation of the radicals. These assumptions are very plausible because no population differences can be generated until the radicals have separated to r_0, and the other components of the density matrix are destroyed during the time needed to reach that distance; this effect must become stronger for increasing Coulombic attraction between the radicals because their separation is slowed. Simulations indicate that for typical parameters this approximation is indeed excellent.

The excursion is assumed to end at the encounter distance d ($d < r_0$). This will slightly overestimate the population difference generated, because the time spent inside the exchange region is wrongly counted as productive for creating a population difference, and the loss of phase correlation on a trajectory that crosses the exchange region without leading to an encounter is not taken into account. To overcome this dissymmetry of the Freed−Pedersen theory, a refined reencounter model has been proposed,[9] to which the results of this paper should be applicable without modification. In the case of a Coulombic attraction between the radicals the dissymmetry is less severe because once the radicals have entered the exchange region, rapid termination of the diffusional excursion is much more probable than for freely diffusing radicals. Again, this reasoning is borne out by simulations of trajectories.

Solution of eq 1 under the described conditions is straightforward. Provided that the probability density of first reencounter $f(t,d|r_0)$ is known, an average over the trajectories can then be performed, which leads to the following relationship between the density matrixes before and after each member of the ensemble has undergone one diffusional excursion

$$\begin{pmatrix}\overline{\rho_{SS}-\rho_{T_0T_0}}\\ \overline{2\mathrm{Im}(\rho_{ST_0})}\\ \overline{2\mathrm{Re}(\rho_{ST_0})}\end{pmatrix}_{\mathrm{after}}=\begin{pmatrix}c & -s & 0\\ s & c & 0\\ 0 & 0 & p\end{pmatrix}\cdot\begin{pmatrix}\overline{\rho_{SS}-\rho_{T_0T_0}}\\ \overline{2\mathrm{Im}(\rho_{ST_0})}\\ \overline{2\mathrm{Re}(\rho_{ST_0})}\end{pmatrix}_{\mathrm{before}} \quad (3)$$

The quantities c and s are the Fourier cosine and sine transforms at the angular frequency of intersystem crossing $2Q/\hbar$, and p is the total probability of first reencounter,

$$c=\int_0^\infty f(t,d|r_0)\cos(2Q/\hbar)\mathrm{d}t \quad (4)$$

$$s=\int_0^\infty f(t,d|r_0)\sin(2Q/\hbar)\mathrm{d}t \quad (5)$$

$$p=\int_0^\infty f(t,d|r_0)\mathrm{d}t \quad (6)$$

Analytical expressions for p are known for all relevant circumstances (see below).

On the basis of eqs 3−6, the yield of geminate products can be computed for each nuclear spin state. If electron spin polarization and phase correlation are destroyed upon each reencounter (see above), if the radical pair starts out in state $|T_0\rangle$, and if the probability of geminate reaction in the singlet state is unity, this yield F^* is given by[1d]

$$F^*=\frac{p-c}{2-p+c} \quad (7)$$

For any other initial condition or reaction probability, the

geminate yield can also be computed from F^* in a very simple way, needing only the spin independent reaction probability as an additional parameter.[3b]

These further calculations are outside the scope of this work, which focuses on the conditional probability density $f(t,d|r_0)$ in the case of a Coulombic interaction between the radicals and its Fourier transforms c and s, i.e., on the central diffusion-related quantities needed to obtain absolute CIDNP intensities for radical ion pairs.

Computer Simulation Method. The principle of our calculations was straightforward: For each set of diffusional and electrostatic parameters, an ensemble of identical radical pairs was considered. Individual trajectories of the ensemble members under the combined influence of randomly chosen discrete steps and directed electrostatic drift were simulated. The durations of these trajectories were collected in a histogram, which directly gives the probability density of a first reencounter of the radicals.

Each step of duration Δt consisted of the superposition of a random displacement of constant length x,

$$x = \sqrt{6D\Delta t} \tag{8}$$

where D is the diffusion coefficient, and a linear motion Δr

$$\Delta r = \mu E \Delta t \tag{9}$$

with the mobility μ and the electric field E (drift-field approximation).[10] Only Coulombic attraction is considered in this paper, because CIDNP experiments on radical ion pairs exhibiting Coulombic repulsion do not seem to have been done so far. Hence, the displacement Δr is always negative. In contrast, the random vector of length x adds vectorially to the vector connecting the two radicals of a pair. With eq 8 and the usual expressions for μ and E, eq 9 can be rewritten as

$$\Delta r = -\frac{r_c x^2}{6\overline{r^2}} \tag{10}$$

where r_c is the Onsager radius,

$$r_c = \frac{e^2}{4\pi\epsilon_0\epsilon_r kT} \tag{11}$$

and the mean distance $\overline{r^2}$ is obtained by

$$\frac{1}{\overline{r^2}} = \left(\frac{1}{r_{old}^2} + \frac{1}{r_{new}^2}\right)/2 \tag{12}$$

from the distances r_{old} and r_{new} before and after the random step.

In the absence of geometrical constraints, such as those found in micelles, the situation of a pair $\overline{AB}$ at time t during a diffusional excursion is completely described by the distance $r(t)$ between the radicals. It is thus sufficient to regard radical A as stationary and radical B as moving with the interdiffusion coefficient D and the sum of the ionic mobilities of the two radicals.

To model the isotropic diffusional steps of B we chose the inverse distribution function method,[11] because this clearly provides a computationally more efficient approach than the von Neumann rejection technique under the circumstances. Let B undergo a diffusional displacement of constant length x but

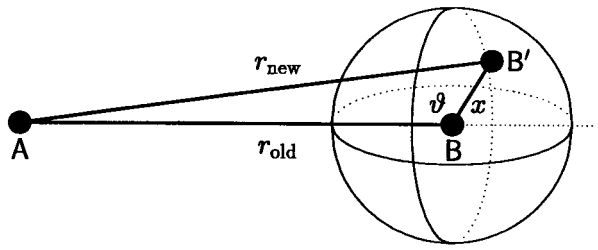

Figure 1. Isotropic diffusional step of length x of a radical pair $\overline{AB}$. The figure illustrates the relationship between the interradical separation before and after the step, r_{old} and r_{new}. For further explanation, see text.

arbitrary orientation in space, which takes it to position B′ (Figure 1). The points A, B, and B′ form a triangle, so

$$r_{new} = \sqrt{r_{old}^2 + x^2 - 2r_{old}x\cos\vartheta} \tag{13}$$

The A−B−B′-angle ϑ is not uniformly distributed between 0 and π because B′ is constrained to lie on a sphere of radius x around B. By integrating the surface element $x^2 \sin\vartheta\, d\vartheta\, d\varphi$ over the angle φ, which is uniformly distributed between 0 and 2π, one arrives at the normalized probability density $p(\vartheta)$

$$p(\vartheta)d\vartheta = \frac{x^2 \sin\vartheta\, d\vartheta \int_0^{2\pi} d\varphi}{x^2 \int_0^{\pi} \sin\vartheta\, d\vartheta \int_0^{2\pi} d\varphi} = 0.5 \sin\vartheta\, d\vartheta \tag{14}$$

Hence, the distribution function $F(\Theta)$ is

$$F(\Theta) = \int_0^{\Theta} p(\vartheta)d\vartheta = 0.5(1 - \cos\Theta) \tag{15}$$

The desired distribution of angles is obtained by inverting eq 15,

$$\Theta = \arccos(1 - 2z) \tag{16}$$

where z is a random number distributed uniformly between 0 and 1. Insertion of this result into eq 13 finally yields

$$r_{new} = \sqrt{r_{old}^2 + x^2 - r_{old}[x(2 - 4z)]} = \sqrt{r_{old}^2 + x^2 - r_{old}w} \tag{17}$$

Thus, a diffusional step of B that is uniformly distributed on the surface of a sphere of radius x can be modeled in a very simple way with a random number w distributed uniformly in the interval $-2x \le w \le +2x$. No calculation of trigonometric functions is necessary, so the algorithm is quite fast.

The diffusional steps modify r, and thus the Coulombic attraction. Hence, drift and diffusion are coupled. Their separation by the drift-field approximation is only permissible if the perturbation of the ionic drift by the diffusional steps is small. Following arguments in the literature[12] we take "small" to mean that the potential energy does not change by more than kT during a diffusional step. The largest effect is found when r decreases by x, so this condition is always fulfilled if we let

$$-\frac{e^2}{4\pi\epsilon_0\epsilon_r}\left(\frac{1}{r} - \frac{1}{r - x}\right) < kT \tag{18}$$

For $x < r$, which is expected to hold, insertion of eq 11 yields

$$x/r < 1/(1 + r_c/r) \tag{19}$$

The lower limit of the right-hand side of this expression is found for the smallest possible value of r, i.e., $r = d$, where d is the

encounter distance. Therefore, we chose

$$x/r < 1/(1 + r_c/d) \tag{20}$$

As eq 20 shows, a small value of x must be used when the radicals of a pair reside near one another. However, for large separations this is not only unnecessary but also computationally inefficient. Therefore, x was scaled linearly with the interradical distance, which is equivalent to scaling the time intervals of the individual diffusional steps with r^2. This greatly reduces the time needed to simulate a diffusional excursion while maintaining the condition for the validity of the drift-field approximation, eq 20.

Reduced variables, symbolized by a tilde, "$\sim$", were employed throughout. For this, all lengths were divided by the encounter distance d, and times were multiplied by $6D/d^2$ (compare eq 8).

For an estimation of the parameter range relevant for the simulations, a value of 6 Å (this is slightly less than the mean size of a single benzene molecule taking into account the van der Waals radii) was chosen as fairly typical for d of an organic radical ion pair. The Onsager radius at room temperature is 558 Å/ϵ_r. Simulations were performed up to $\tilde{r}_c = 16$, which would include solvents with a relative permittivity ϵ_r as low as 6.

In accordance with eq 20, the ratio x/r was, therefore, normally set to 1/20. By carrying out additional simulations with a smaller ratio, the dependence of the obtained probability density on this ratio was checked. Slight discrepancies, in particular superimposed weak oscillations in the early parts of the curves, arose when the starting distance r_0 approached d (for $\tilde{r}_0 < 1.4$), which could be removed by reducing x/r to 1/50 in these cases. Because these effects were also observed in the absence of Coulombic interactions, they were obviously not due to a breakdown of the drift-field approximation but were artifacts caused by the discretization of the isotropic diffusional step. Because with the Freed−Pedersen model the starting distance is equal to the distance where the exchange interaction has decreased to a negligible level, a value of 1.1 was chosen as the minimum $\tilde{r}_0$, which should include even extremely weak exchange interaction. Simulations were performed up to a maximum value of $\tilde{r}_0$ of 4.

A computed trajectory terminated either when r became smaller than or equal to d, or when no reencounter had occurred after a given time limit t_{max}. We took $6Dt_{max}/d^2$ to be 3×10^6. Assuming a typical interdiffusion coefficient of 4×10^{-5} cm^2 s^{-1} this corresponds to an actual time on the order of 50 μs. This second end criterion, which had to be invoked only for small $\tilde{r}_c$ and large $\tilde{r}_0$, takes into account that the contributions of excessively long diffusional excursions to CIDNP should be quite small, because nuclear spin polarizations are lost by relaxation. Besides, comparisons of the obtained total probabilities of reencounter with the analytical solutions (see below) indicated that most of these excursions would not have led to a reencounter anyway.

Random numbers were generated with a subtractive algorithm and a subsequent randomizing shuffle to remove any sequential correlations.[11] To ensure statistical behavior, the system time was used for initialization before each run. Typically, an ensemble of radical pairs comprised between 1 and 10 million members. Calculation of their trajectories took about an hour on a Pentium-III PC.

Two independent tests of the validity of the simulation procedure were available. First, for $\tilde{r}_c = 0$, i.e., in the absence of Coulombic interactions, an analytical solution of the conditional probability density of first reencounter exists,[5] which in reduced units is given by

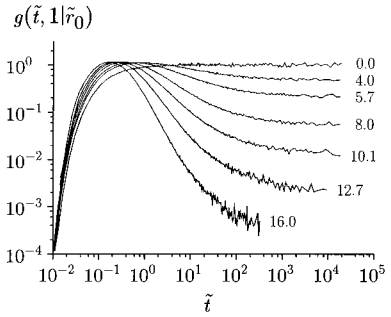

Figure 2. Time dependence of the modified probability density $g(\tilde{t},1|\tilde{r}_0)$ (see eq 23) for constant $\tilde{r}_0$, $\tilde{r}_0 = 1.26$, and variable Onsager radius $\tilde{r}_c$ (given at the traces).

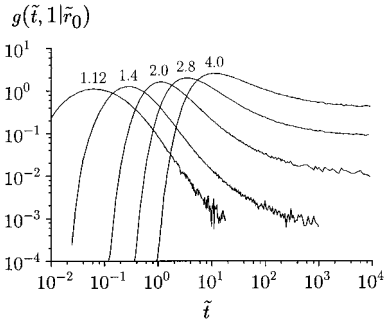

Figure 3. Function $g(\tilde{t},1|\tilde{r}_0)$ (see eq 23) for constant Onsager radius, $\tilde{r}_c = 16$. The parameters at the curves denote the starting distance $\tilde{r}_0$.

$$f(t,d|r_0)\mathrm{d}t = f(\tilde{t},1|\tilde{r}_0)\mathrm{d}\tilde{t} = \frac{\tilde{r}_0 - 1}{\tilde{r}_0}\sqrt{\frac{3}{2\pi}}\,\tilde{t}^{-3/2}\exp\left[-\frac{3(\tilde{r}_0 - 1)^2}{2\tilde{t}}\right]\mathrm{d}\tilde{t} \tag{21}$$

Second, the total probability of reencounter of pairs with a Coulombic interaction between the radicals, is[13]

$$p = \int_0^\infty f(t, d|r_0)\mathrm{d}t = \frac{1 - \exp(-r_c/r_0)}{1 - \exp(-r_c/d)} = \frac{1 - \exp(-\tilde{r}_c/\tilde{r}_0)}{1 - \exp(-\tilde{r}_c)} \tag{22}$$

which reduces to the known expression for free diffusion[5] $p = d/r_0 = \tilde{r}_0^{-1}$ in the limit of vanishing Coulombic interaction. The simulation results were found to agree excellently with all these analytical results.

Probability Densities of First Reencounter and Their Transforms. The changes in $f(\tilde{t},1|\tilde{r}_0)$ caused by a Coulombic interaction are best seen when the curves are divided by the time-independent factor and the $\tilde{t}^{-3/2}$ term of the expression for free diffusion, eq 21. In Figure 2, the resulting functions $g(\tilde{t},1|\tilde{r}_0)$,

$$g(\tilde{t},1|\tilde{r}_0) = f(\tilde{t},1|\tilde{r}_0)\frac{\tilde{r}_0}{\tilde{r}_0 - 1}\sqrt{\frac{2\pi}{3}}\tilde{t}^{+3/2} \tag{23}$$

have been plotted for constant starting distance $\tilde{r}_0$ but different Onsager radii $\tilde{r}_c$. Figure 3 shows the same type of plot for constant $\tilde{r}_c$ and variable $\tilde{r}_0$. It is found that each curve $g(\tilde{t},1|\tilde{r}_0)$ converges toward a constant value, so the presence of the Coulombic interaction does not change the long-term behavior ($t^{-3/2}$ dependence) of $f(\tilde{t},1|\tilde{r}_0)$. The asymptotic value depends on both $\tilde{r}_0$ and $\tilde{r}_c$.

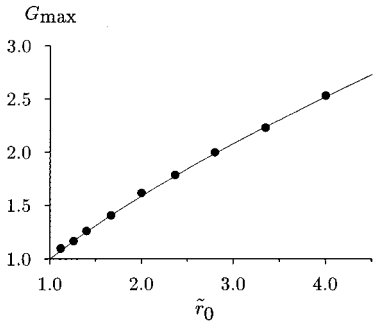

Figure 4. Dependence of the maximum value $G_{\max}$ of the modified probability density $g(\tilde{t},1|\tilde{r}_0)$ (eq 23) on the initial radical separation $\tilde{r}_0$. The solid line is the fit curve $\tilde{r}_0^{2/3}$.

From these figures, it is evident that all curves $g(\tilde{t},1|\tilde{r}_0)$ except that for $\tilde{r}_c = 0$ (no Coulombic interaction) pass through a maximum, the height of which is practically insensitive to $\tilde{r}_c$ but exhibits a weak dependence on $\tilde{r}_0$: To a very good approximation, this maximum height is proportional to $\tilde{r}_0^{2/3}$, as can be seen in Figure 4. With increasing Coulombic attraction, the position of the maximum shifts toward earlier times, which is physically plausible because it reflects the distance-dependence of the Coulombic interaction, short times corresponding to small separations (eq 8). However, the position of the maximum exhibits a much stronger dependence on $\tilde{r}_0$ than on $\tilde{r}_c$.

Furthermore, as Figure 3 shows, and closer inspection also reveals for Figure 2, at times well before the maximum the curves $g(\tilde{t},1|\tilde{r}_0)$ are related to one another by horizontal displacements in the log−log plots. This would be consistent with expressions of the general form $\exp(b\tilde{t}^q)$, of which the result in the absence of Coulombic interaction, $\exp(-a/\tilde{t})$, is a special case. However, the time-dependent part of $g(\tilde{t},1|\tilde{r}_0)$ must comprise another time-dependent factor, because $\exp(b\tilde{t}^q)$ is a monotonic function of $\tilde{t}$. The horizontal shifts are only very weakly dependent on $\tilde{r}_c$ (compare Figure 2) but show a pronounced dependence on $\tilde{r}_0$ (see Figure 3). Most of the latter effect is also present in the case of free diffusion, where two curves $g(\tilde{t},1|\tilde{r}_{0,a})$ and $g(\tilde{t},1|\tilde{r}_{0,b})$ would be horizontally displaced by $[(\tilde{r}_{0,a} - 1)/(\tilde{r}_{0,b} - 1)]^2$ in a log−log plot. The actual displacements in Figure 3 are always smaller than the value expected for free diffusion, and show a systematic deviation that increases with decreasing $\tilde{r}_0$ (2% when going from $\tilde{r}_0 = 4.0$ to $\tilde{r}_0 = 2.8$ compared to 12% when going from $\tilde{r}_0 = 2.0$ to $\tilde{r}_0 = 1.4$ in Figure 3).

Attempts to approximate $f(\tilde{t},1|\tilde{r}_0)$ by suitable functions, guided by these observations, would certainly be successful. However, we found it more promising to approximate the Fourier cosine and sine transforms of $f(\tilde{t},1|\tilde{r}_0)$, c and s, because these are the quantities needed for calculation of absolute CIDNP intensities.

Because time is measured in reduced units in our simulations, the numerical Fourier transformation of $f(\tilde{t},1|\tilde{r}_0)$ yields functions of reduced frequencies $\tilde{\nu}$ that are obtained by multiplying the actual frequencies with $d^2/(6D)$. To estimate the relevant range of $\tilde{\nu}$, one may assume that the mixing matrix element Q (eq 2) is dominated by the Zeeman term. A value of 10^{-3} appears fairly typical for Δg of organic radicals, and a value of 10^{-2} will hardly ever be surpassed. For a CIDNP experiment run on a 500 MHz NMR spectrometer, one thus has an angular frequency of intersystem crossing between 10^9 and 10^{10} s^{-1}, so with the above assumptions for d and D, $2\pi\tilde{\nu}_{\max}$ is expected to lie between 0.03 and 0.3.

In the absence of Coulombic interactions, the conditional probability density of first reencounter (see eq 21) can be transformed analytically. In reduced units, the results are[3b]

$$c_{\tilde{r}_c=0} = p \exp(-z) \cos(z) \tag{24}$$

$$s_{\tilde{r}_c=0} = \mathrm{sgn}(Q) p \exp(-z) \sin(z) \tag{25}$$

where

$$z = (\tilde{r}_0 - 1)\sqrt{6\pi|\tilde{\nu}|} \tag{26}$$

and the reduced intersystem crossing frequency $\tilde{\nu}$ is given by $|Q|d^2/(3Dh)$.

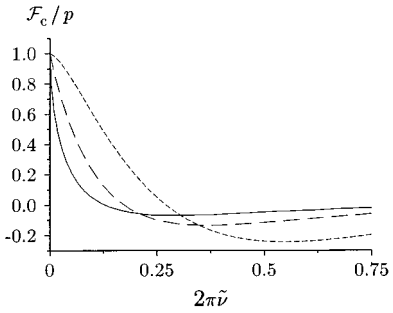

Figure 5. Normalized Fourier cosine transforms $\mathcal{F}_c/p$ of the probability density of first reencounter as functions of the reduced frequency for constant initial separation ($\tilde{r}_0 = 2$) and different Onsager radii: solid line, $\tilde{r}_c = 0$; long dashed line, $\tilde{r}_c = 8$; short dashed line, $\tilde{r}_c = 16$.

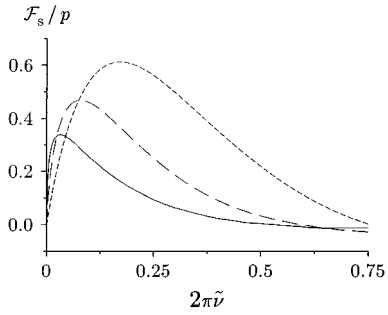

Figure 6. Normalized Fourier sine transforms $\mathcal{F}_s/p$ of the probability density of first reencounter as functions of the reduced frequency for constant initial separation ($\tilde{r}_0 = 2$) and different Onsager radii: solid line, $\tilde{r}_c = 0$; long dashed line, $\tilde{r}_c = 8$; short dashed line, $\tilde{r}_c = 16$.

In Figures 5 and 6, examples of the numerically obtained Fourier cosine and sine transforms of the simulated probability densities $f(\tilde{t},1|\tilde{r}_0)$ have been plotted for different Onsager radii. Because the complex Fourier transform of $f(\tilde{t},1|\tilde{r}_0)$ for $\tilde{\nu} = 0$ is equal to p (cf eqs 4−6), it is clear that both transforms must contain the total probability of reencounter p as a multiplicative factor. Hence, for comparison all transforms were divided by p (eq 22).

Inspection of the resulting curves shows that their general features are not influenced by a Coulombic attraction between the radicals: They all display an oscillatory behavior, with maxima, minima, and zero crossings of the sine and cosine transforms interleaved in exactly the same way as in the case of free diffusion. The distances between these characteristic points are seen to be nonlinear functions of $\tilde{\nu}$, and to depend on both $\tilde{r}_0$ and $\tilde{r}_c$. In the next section, we use these properties to derive suitable model functions for the transforms.

Approximations for the Cosine and Sine Transforms. On the grounds of the preceding observations, we assume that the general functional forms of the transforms remain unchanged by a Coulombic interaction but that the argument functions change. Hence, as model functions for the cosine and sine

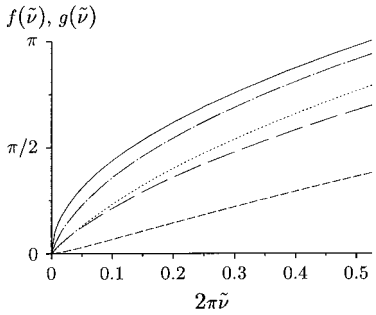

Figure 7. Argument functions (see eqs 27 and 28) obtained from the numerical transforms shown in Figures 5 and 6 with eqs 29 and 30. For all curves, $\tilde{r}_0$ is 2. Solid line, $f(\tilde{\nu})$ and $g(\tilde{\nu})$ for $\tilde{r}_c = 0$; long dashed line, $f(\tilde{\nu})$ for $\tilde{r}_c = 8$; dashed−dotted line, $g(\tilde{\nu})$ for $\tilde{r}_c = 8$; short dashed line, $f(\tilde{\nu})$ for $\tilde{r}_c = 16$; dotted line, $g(\tilde{\nu})$ for $\tilde{r}_c = 16$.

transforms, $\mathcal{F}_{c,model}$ and $\mathcal{F}_{s,model}$, we take

$$\mathcal{F}_{c,model} = p \exp[-f(\tilde{\nu})] \cos[g(\tilde{\nu})] \tag{27}$$

$$\mathcal{F}_{s,model} = \mathrm{sgn}(Q) p \exp[-f(\tilde{\nu})] \sin[g(\tilde{\nu})] \tag{28}$$

where the argument function of the exponential term $f(\tilde{\nu})$ and that of the trigonometric function $g(\tilde{\nu})$ is *the same in both transforms*. The first argument function follows from the numerically obtained cosine and sine transforms $\mathcal{F}_c$ and $\mathcal{F}_s$ in a straightforward way,

$$f(\tilde{\nu}) = -\ln[(\mathcal{F}_c/p)^2 + (\mathcal{F}_s/p)^2]/2 \tag{29}$$

whereas $g(\tilde{\nu})$ is a piecewise function. For our approximations, we restricted $\tilde{\nu}$ to the range from 0 to the first zero crossing of $\mathcal{F}_s$, which usually occurs at much higher values than $\tilde{\nu}_{max}$ estimated in the preceding section. Under these circumstances, $g(\tilde{\nu})$ is given by

$$g(\tilde{\nu}) = \begin{cases} \mathrm{arccot}\,(\mathcal{F}_c/\mathcal{F}_s) & : \ \mathcal{F}_c \geq 0 \\ \mathrm{arccot}\,(\mathcal{F}_c/\mathcal{F}_s) + \pi & : \ \mathcal{F}_c < 0 \end{cases} \tag{30}$$

Examples of the resulting argument functions have been plotted in Figure 7.

The known analytical results (eqs 24−26) show that in the case of free diffusion $f(\tilde{\nu})$ and $g(\tilde{\nu})$ are identical, and their functional form is a proportionality to $\tilde{\nu}^{1/2}$. Figure 7 reveals that the presence of a Coulombic interaction causes these two functions to become nondegenerate, the differences between them increasing with increasing $\tilde{r}_c$, and the exponent to become larger than 1/2. Hence, model functions for $f(\tilde{\nu})$ and $g(\tilde{\nu})$, f_{model} and g_{model}, were expressed as

$$f_{model}(\tilde{\nu}) = [a(\tilde{r}_0, \tilde{r}_c)\tilde{\nu}]^{m(\tilde{r}_0,\tilde{r}_c)} \tag{31}$$

$$g_{model}(\tilde{\nu}) = [b(\tilde{r}_0, \tilde{r}_c)\tilde{\nu}]^{n(\tilde{r}_0,\tilde{r}_c)} \tag{32}$$

With $f(\tilde{\nu})$ and $g(\tilde{\nu})$ obtained from eqs 29 and 30, plots of $\ln[f(\tilde{\nu})]$ and $\ln[g(\tilde{\nu})]$ as functions of $\tilde{\nu}$ indeed gave straight lines, with very small deviations from linearity only, so eqs 31 and 32 appear to be quite good approximations.

For each set of $\tilde{r}_0$ and $\tilde{r}_c$, separate linear least-squares fits of $\mu \ln(\tilde{\nu})$ to $\ln[f(\tilde{\nu})]$ and to $\ln[g(\tilde{\nu})]$ gave starting values of a and m, and b and n, respectively. However, instead of minimizing χ^2 between the actual and the approximate argument functions (i.e., between eqs 29 and 31 as well as eqs 30 and 32), one should minimize χ^2 between the calculated transforms $\mathcal{F}_c$ and $\mathcal{F}_s$ of the Monte Carlo results and the approximated transforms obtained by inserting eqs 31 and 32 into eqs 27 and 28. Therefore, in a second step, the parameter sets were refined by simultaneous nonlinear fits of these approximated transforms to $\mathcal{F}_c$ and $\mathcal{F}_s$, using the simplex algorithm given in ref 11. Because smaller values of $\tilde{\nu}$ are most frequently encountered, the first part of the data, up to the maximum of the sine transform, was given twice the weight of the later part of the data in these fits. The differences between the model curves obtained in this way and $\mathcal{F}_c$ and $\mathcal{F}_s$ were found to be very small.

To express a, b, m, and n as functions of $\tilde{r}_0$ and $\tilde{r}_c$, the resulting array of parameters was first partitioned into sets of constant $\tilde{r}_0$, and the dependence on $\tilde{r}_c$ was analyzed for each set. In the absence of a Coulombic interaction, the exponents m and n are equal to 1/2 and the terms a and b are both given by $6\pi(\tilde{r}_0 - 1)^2$, as eqs 24 and 25 show. Hence, functions of the general form $1/2 + \phi(\tilde{r}_0, \tilde{r}_c)$ for m and n, and $6\pi(\tilde{r}_0 - 1)^2\psi(\tilde{r}_0, \tilde{r}_c)$ for a and b were chosen as the most promising candidates. It was found that for each set the deviations of the exponents m and n from 1/2 were to a very good approximation directly proportional to $\tilde{r}_c$, and the multiplicative factors ψ in a and b were well describable by expressions of the type $A^{-B\tilde{r}_c}$. Next, the dependence on $\tilde{r}_0$ of the constant of proportionality C in the former case and of A and B in the latter was investigated. This analysis revealed that A, B, and C can be represented very well by $\alpha \ln(\tilde{r}_0)$, $\beta/\tilde{r}_0$, and $\gamma \ln(\tilde{r}_0)/\tilde{r}_0^2$, respectively.

Thus, good approximations of $\mathcal{F}_c$ and $\mathcal{F}_s$ are provided by

$$\mathcal{F}_c(\tilde{r}_0, \tilde{r}_c) \approx p \exp[-u(\tilde{r}_0, \tilde{r}_c, \alpha_1, \beta_1)\tilde{\nu}]^{\upsilon(\tilde{r}_0,\tilde{r}_c,\gamma_1)} \cos[u(\tilde{r}_0, \tilde{r}_c, \alpha_2, \beta_2)\tilde{\nu}]^{\upsilon(\tilde{r}_0,\tilde{r}_c,\gamma_2)} \tag{33}$$

$$\mathcal{F}_s(\tilde{r}_0, \tilde{r}_c) \approx \mathrm{sgn}(Q) p \exp[-u(\tilde{r}_0, \tilde{r}_c, \alpha_1, \beta_1)\tilde{\nu}]^{\upsilon(\tilde{r}_0,\tilde{r}_c,\gamma_1)} \sin[u(\tilde{r}_0, \tilde{r}_c, \alpha_2, \beta_2)\tilde{\nu}]^{\upsilon(\tilde{r}_0,\tilde{r}_c,\gamma_2)} \tag{34}$$

with

$$u(\tilde{r}_0, \tilde{r}_c, \alpha, \beta) = 6\pi(\tilde{r}_0 - 1)^2(\alpha\tilde{r}_0)^{-(\beta\tilde{r}_c)/\tilde{r}_0} \tag{35}$$

$$\upsilon(\tilde{r}_0, \tilde{r}_c, \gamma) = 1/2 + \gamma\frac{\ln(\tilde{r}_0)}{\tilde{r}_0^2}\tilde{r}_c \tag{36}$$

and can be expressed in terms of six parameters, one set of three for the exponential term and another set of three for the trigonometric terms.

Finally, starting values of the six constants were obtained by fitting the argument functions (u and υ in eqs 31 and 32, with eqs 35 and 36) to the array of a, m, b, and n, and then refined by a global nonlinear fit of eqs 33 and 34 to all data sets $\mathcal{F}_c$ and $\mathcal{F}_s$. Rather than carrying out a brute-force fit, the following approach was chosen to minimize the absolute deviations: Errors of a, m, b, and n in eqs 31 and 32 propagate to $\mathcal{F}_{c,model}$ and $\mathcal{F}_{s,model}$ according to

$$\frac{\partial\mathcal{F}_{c,model}}{\partial a} = -(m/a)(a\tilde{\nu})^m\mathcal{F}_{c,model} \tag{37}$$

$$\frac{\partial\mathcal{F}_{s,model}}{\partial a} = -(m/a)(a\tilde{\nu})^m\mathcal{F}_{s,model} \tag{38}$$

$$\frac{\partial\mathcal{F}_{c,model}}{\partial m} = -(a\tilde{\nu})^m\ln(a\cdot\tilde{\nu})\mathcal{F}_{c,model} \tag{39}$$

$$\frac{\partial \mathcal{F}_{\mathrm{s,model}}}{\partial m} = -(a\tilde{\nu})^m \ln(a\cdot\tilde{\nu})\mathcal{F}_{\mathrm{s,model}} \tag{40}$$

$$\frac{\partial \mathcal{F}_{\mathrm{c,model}}}{\partial b} = -(n/b)(b\tilde{\nu})^n \mathcal{F}_{\mathrm{s,model}} \tag{41}$$

$$\frac{\partial \mathcal{F}_{\mathrm{s,model}}}{\partial b} = (n/b)(b\tilde{\nu})^n \mathcal{F}_{\mathrm{c,model}} \tag{42}$$

$$\frac{\partial \mathcal{F}_{\mathrm{c,model}}}{\partial n} = -(b\tilde{\nu})^n \ln(b\cdot\tilde{\nu})\mathcal{F}_{\mathrm{s,model}} \tag{43}$$

$$\frac{\partial \mathcal{F}_{\mathrm{s,model}}}{\partial n} = (b\tilde{\nu})^n \ln(b\cdot\tilde{\nu})\mathcal{F}_{\mathrm{c,model}} \tag{44}$$

On the basis of the preceding equations, those four points of each curve $\mathcal{F}_c$ and $\mathcal{F}_s$ were chosen, for which deviations of the parameters have the largest effect, and the global fit procedure was then carried out for the resulting data sets of eight per pair ($\tilde{r}_0$, $\tilde{r}_c$). The best-fit result,

$$\alpha_1 = 1.1767 \qquad \alpha_2 = 0.9734 \tag{45}$$

$$\beta_1 = 0.3106 \qquad \beta_2 = 0.1837 \tag{46}$$

$$\gamma_1 = 0.1771 \qquad \gamma_2 = 0.0948 \tag{47}$$

gives a maximum error of less than 0.06, i.e., 6% of the maximum value of $\mathcal{F}_c$ or $\mathcal{F}_s$ in the experimentally realistic range of frequencies ($2\pi\tilde{\nu} \leq 0.3$, see above). With decreasing $\tilde{r}_c$ and increasing $\tilde{r}_0$, the error becomes smaller. Figure 8 shows the deviations of the approximations from the numerically obtained Fourier cosine and sine transforms in the worst-case ($\tilde{r}_c = 16$, $\tilde{r}_0 = 1.12$), and Figure 9 illustrates the dependence of the maximum errors on $\tilde{r}_0$. From the latter figure, it can be inferred that the approximation of the cosine transform, which is the quantity needed for calculating CIDNP intensities (eq 7), remains good even for $\tilde{r}_0 \rightarrow 1$.

Comparisons of the approximations and the numerical transforms reveal that all the deviations are in fact horizontal distortions, which is also to be expected because they are due to errors in the argument functions. Given the fact that usually the magnetic and diffusional parameters of the radicals are not known to a very high degree of precision, i.e., that $\tilde{\nu}$ is somewhat uncertain, the errors of these approximations thus appear quite tolerable. Furthermore, for small argument functions, a first-order expansion of eq 27 can be performed. By carrying out the analogous calculations as in the case of free diffusion[3b] one finds that the quantity F^* (eq 7) is given by

$$F^* = \frac{pf(\tilde{\nu})}{2(1-p)} \tag{48}$$

in this limit. On one hand, Figure 7 shows that in the presence of a Coulombic attraction between the radicals this simplified form is valid over a much wider range of $\tilde{\nu}$ than in the case of free diffusion. On the other hand, as the argument function $f(\tilde{\nu})$ is approximated with smaller deviations than is $\exp[-f(\tilde{\nu})]$, the errors in the CIDNP signals are even smaller than expected from Figure 9.

To illustrate an application of the results derived in this paper, we calculate the dependence of CIDNP intensities on the relative permittivity ϵ_r of the solvent. As model system, we choose a radical ion pair with a g value difference of 2×10^{-4} containing one proton (hyperfine coupling constant 20 G) and possessing the diffusional parameters $d = 6$ Å, $D = 4 \times 10^{-5}$ cm^2 s^{-1}, and $\tilde{r}_0 = 1.4$. From ϵ_r, $\tilde{r}_c$ is obtained with eq 11, which in turn yields p (eq 22). With the frequency $\tilde{\nu}$, which follows from the magnetic and diffusional parameters and the proton spin state, the cosine transform $\mathcal{F}_c$ is computed with eqs 45−47, 35−36, and 33. By inserting this result and the value of p into eq 7 one gets F^*. Finally, this calculation is performed for the α and the β spin state of the proton, and subtraction gives the population difference, which is directly proportional to the CIDNP signal. The curve obtained in this way (Figure 10) agrees quite well with the experimentally observed[14] dependence of CIDNP intensities on ϵ_r. In particular, its general shape reproduces the experimental data much better than does the numerical simulation in ref 14.

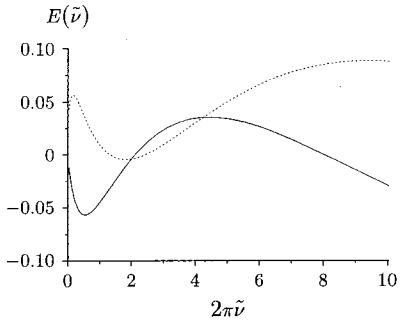

Figure 8. Worst-case ($\tilde{r}_0 = 1.12$, $\tilde{r}_c = 16$) deviations $E(\tilde{\nu})$ of the approximations of $\mathcal{F}_c$ and $\mathcal{F}_s$ from the numerical Fourier transforms of the Monte Carlo results. Solid line, cosine transform; dotted line, sine transform. The frequency range in this figure—up to the first zero crossing of $\mathcal{F}_s$—is much greater than is experimentally relevant (see text).

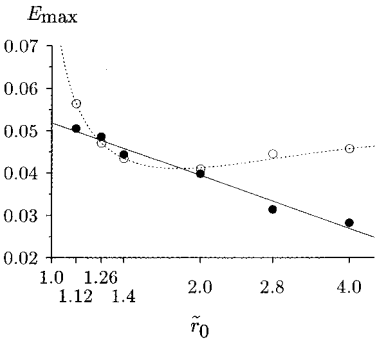

Figure 9. Dependence of the maximum approximation errors E_{max} of $\mathcal{F}_c$ (solid circles) and $\mathcal{F}_s$ (open circles) on the starting distance $\tilde{r}_0$ for $\tilde{r}_c = 16$. The solid line is a linear regression, the broken line is a polynomial fit, which has no significance for $\tilde{r}_0 \leq 1.12$.

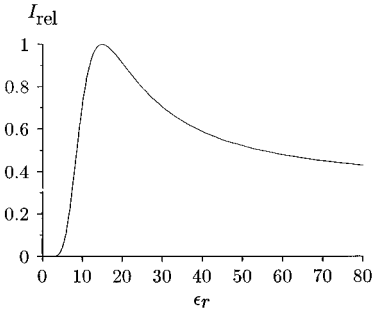

Figure 10. Calculation of normalized CIDNP signal intensities I_{rel} as functions of the relative solvent permittivity ϵ_r for a model system. Further explanation, see text.

Conclusions

It has been shown that six constants (eqs 45−47) suffice to reproduce the Fourier transforms $\mathscr{F}_c$ and $\mathscr{F}_s$ throughout a wide range of diffusional parameters ($1.1 \leq \tilde{r}_0 \leq 4$ and $0 \leq \tilde{r}_c \leq 16$) very satisfactorily by the functions of eqs 33−36 despite the comparatively simple form of the latter. Attempts to extend the described methods to constrained diffusion, e.g., in micellar systems, are in progress.

References and Notes

(1) For instance, see: (a) Muus, L. T., Atkins, P. W., McLauchlan, K. A., Pedersen, J. B., Eds. *Chemically Induced Magnetic Polarization*; D. Reidel: Dordrecht, 1977. (b) Salikhov, K. M.; Molin, Yu. N.; Sagdeev, R. Z.; Buchachenko, A. L. *Spin Polarization and Magnetic Effects in Radical Reactions*; Elsevier: Amsterdam, 1984. (c) Steiner, U. E.; Ulrich, T. *Chem. Rev.* **1989**, *89*, 51−147. (d) Goez, M. *Adv. Photochem.* **1997**, *23*, 63−163.

(2) (a) Kaptein, R.; Oosterhoff, L. J. *Chem. Phys. Lett.* **1969**, *4*, 195−197. (b) Closs, G. L. *J. Am. Chem. Soc.* **1969**, *91*, 4552−4554.

(3) (a) Freed, J. H.; Pedersen, J. B. *Adv. Magn. Reson.* **1976**, *8*, 1−84. (b) Pedersen, J. B. *J. Chem. Phys.* **1977**, *67*, 4097−4102.

(4) Noyes, R. M. *J. Am. Chem. Soc.* **1965**, *78*, 5486-5490.

(5) Deutch, J. M. *J. Chem. Phys.* **1972**, *56*, 6076−6081.

(6) Hong, K. M.; Noolandi, J. *J. Chem. Phys.* **1978**, *68*, 5163−5171.

(7) Zharikov, A. A.; Shokhirev, N. V. *Z. Physik. Chem. Neue Folge* **1992**, *177*, 37−61.

(8) See, e.g., Pedersen, J. B.; Lolle, L. I.; Jørgensen, S. *Chem. Phys.* **1992**, *165*, 339−349.

(9) Vollenweider, J.-K.; Fischer, H. *Chem. Phys.* **1988**, *124*, 333−345.

(10) Bartczak, W. M.; Hummel, A. *J. Chem. Phys.* **1987**, *87*, 5222−5228.

(11) Press: W. H.; Flannery, B. P.; Teukolsky, S. A.; Vetterling, W. T. *Numerical Recipes*; Cambridge University Press: Cambridge, 1986.

(12) (a) Williams, F. *J. Am. Chem. Soc.* **1964**, *86*, 3954−3957. (b) Williams, F. *J. Chem. Phys.* **1968**, *48*, 4077−4078.

(13) Mauzerall, D.; Ballard, S. G. *Annu. Rev. Phys. Chem.* **1982**, *33*, 377−407.

(14) Aizawa, T.; Sakata, T.; Itoh, S.; Maeda, K.; Azumi, T. *Chem. Phys. Lett.* **1992**, *195*, 16−20.